RESEARCH

A simple self-assembling system of melittin for hepatoma treatment

Xin Jin[1,2], Qing Yang[1], Guoli Wei[3,4,5], Jie Song[3,4*] and Zhenhai Zhang[3,4*]

*Correspondence:
songjie_pharmacy@163.com;
david23932@163.com

[1] Department of Hospital Pharmacy, Suqian First Hospital, 120 Suzhi Road, Suqian 223800, People's Republic of China
[2] Department of Pharmaceutics, State Key Laboratory of Natural Medicines, China Pharmaceutical University, 24 Tongjiaxiang, Nanjing 210009, China
[3] Affiliated Hospital of Integrated Traditional Chinese and Western Medicine, The Third Clinical Medical College, Nanjing University of Chinese Medicine, Nanjing, Jiangsu, China
[4] Jiangsu Province Academy of Traditional Chinese Medicine, Nanjing, Jiangsu, China
[5] Nanjing Lishui District Hospital of Traditional Chinese Medicine, Nanjing 211200, Jiangsu, China

Abstract

Background: Hepatoma is a serious public health concern. New attempts are urgently needed to solve this problem. Melittin, a host defense peptide derived from the venom of honeybees, has noteworthy hemolysis and non-specific cytotoxicity in clinical applications. Here, the self-assembly of melittin and vitamin E-succinic acid-(glutamate)$_{12}$ (VG) was fabricated via noncovalent π-stacking and hydrogen bonding interactions using an environment-friendly method without "toxic" solvents.

Results: As expected, the designed self-assembly (denoted as M/VG nanoparticles) exhibits a uniform morphology with a particle size of approximately 60 nm and a zeta potential of approximately -26.8 mV. Furthermore, added VG significantly decreased hemolytic activity, increased tumor-targeted effects, and accelerated apoptosis.

Conclusion: Our research provides a promising strategy for the development of natural self-assembled biological peptides for clinical application, particularly for transforming toxic peptides into safe therapeutic systems.

Keywords: Self-assembly, Peptide, Hepatoma therapy, Formation mechanism

Jin *et al. Cancer Nanotechnology*   (2023) 14:2

Page 2 of 14

Graphical Abstract
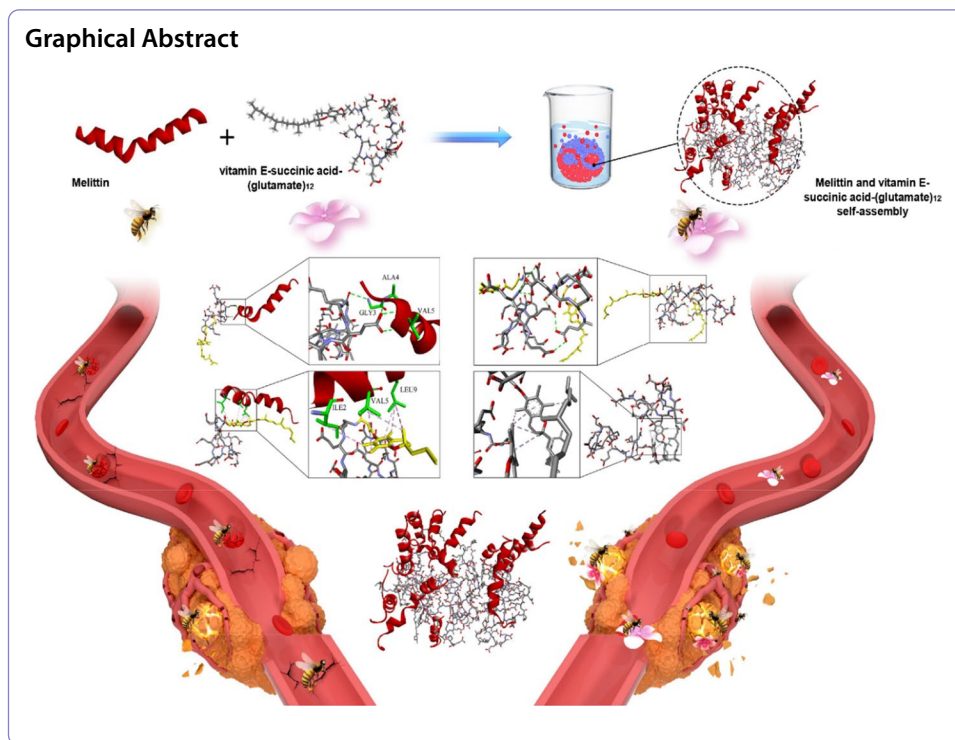
Background

Almost 906,000 new liver cancer cases have been reported, and approximately 830,000 patients die from liver cancer annually, as presented in the global cancer statistics 2020. It is the third most common cancer and is associated with high mortality (Sung et al. 2021). Therefore, it is important to make new attempts to solve this problem. Melittin (GIGAVLKVLTTGLPALISWIKRKRQQ-NH2, M) is the main active pharmacological peptide component of bee venom; it consists of 40–50% of the dry weight of bee venom (Kim 2021). The relative results of a clinical trial of 40 patients with hepatocellular carcinoma treated with melittin for clinical application indicated that the disease control rate was approximately 70% (Mao et al. 2017). Melittin exhibits anti-tumor functions, non-specific cytotoxicity, and non-negligible hemolytic performance.

Two strategies are often used to address these problems. The first is chemical modification to increase specificity and decrease hemolysis (Lyu et al. 2018; Ventura and Wiedman 2021). The second is physicochemical encapsulation by various nanocarriers, such as classical liposomes (Mao et al. 2017), polyelectrolyte nanocarriers (Motiei et al. 2021), polymeric nanocarriers (Lv et al. 2021), redox-sensitive nanocomplexes (Cheng and Xu 2020), pH-sensitive micelles (Peeler et al. 2019), microneedles (Du et al. 2021), inorganic materials (Li et al. 2018), and hydrogels (Zhou et al. 2021a). Modification or complex multifunctional carriers are often limited by the complexity of the production process, high cost, and repeatability, which hinder their clinical applications. Before melittin can be used in the clinic, further investigations are required to maintain a balance between therapeutic benefits, toxicity risks, and preparation technologies (Zhou et al. 2021b).

Self-assembly is a common process in biology, which is the basis for various complex biological structures, such as DNA, microtubules, and vesicles (Lai et al. 2012; Kim and Park 2022). Compared to covalent polymers, peptide-based self-assembly has

advantages such as easy preparation, biodegradability, and biocompatibility (Wang et al. 2021). Moreover, peptide molecules in the blood are usually removed by enzyme degradation, glomerular filtration, and uptake by the reticuloendothelial system (Green et al. 2004). Nevertheless, the self-assembled nanoparticles could provide peptides with high stability, good biological distribution, and tumor-targeted effects, ultimately addressing unmet clinical needs (Chen and Lian 2013; Tu et al. 2007).

Bian et al. recently reported that electrostatic co-assembly behavior exists in oppositely charged small molecules and nanoparticles (Bian et al. 2021). In the present study, we observed the same phenomenon and designed a peptide-assembled nanosystem based on melittin and vitamin E-succinic acid-(glutamate)$_{12}$ (VG) for the treatment of liver cancer. This novel and environment-friendly approach was formed without the use of organic solvents. VG molecules interact with each other to form a hydrophobic core, which interacts with melittin on the surface attached to the core of the nanoparticle through noncovalent π-stacking and hydrogen bonding. The fabricated self-assembled system decreases hemolysis, promotes accumulation in tumors, and increases the dosage of administration in vivo. Compared with free melittin, M/VG nanoparticles could deliver with high does, accumulate in tumor tissues, and exhibit superior anti-tumor effects against HepG2 cells with good biocompatibility.

Materials and methods

Materials
Melittin was synthesized by Nanjing Peptide Industry Biotechnology Co., Ltd. (Nanjing, China). VG was synthesized by China Peptide Industry Biotechnology Co., Ltd. (Shanghai, China). NH_2-Cy5 was purchased from Meilun Biotechnology Co., Ltd. (Dalian, China). HepG2 cells, RPMI-1640 medium, fetal bovine serum, MTT, apoptosis detection kit, and Ki67 detection kit were obtained from KeyGen Biotech Co., Ltd. (Nanjing, China).

Molecular dynamics (MD) simulations
The self-assembly process of the M/VG nanoparticles was analyzed using MD simulations. The PDB ID of melittin is 2mlt. The parameters for the VG molecules were constructed using Amber Tools. An artificial box containing ten melittin and ten VG molecules was designed in a TIP3P water box with a side length of 1 nm. This system was optimized for 5000 steps with 100 ps in the NVT and NPT systems. The temperature was kept constant at 298 K with a relaxation time of 10 ps at 1 bar for a total simulation time of 15 ns. The cutoff distance was 1.2 nm. The simulation time step was 2 fs. MD simulations were performed using the Gaussian09 program based on Gromacs2018.

Preparation and characterization of M/VG nanoparticles
Initially, melittin was added to deionized water to form a solution, then mixed with different ratios of VG (dissolved in buffer solution). The blend was stirred using a magnetic stirrer and further dispersed using bath sonication. Cy5-labeled nanoparticles were prepared as per the above-mentioned technique using Cy5-labeled melittin and VG. To prepare fluorescently labeled melittin, it was conjugated with NH2-Cy5 in accordance with a previous report (Tu et al. 2007).

The negative zeta potentials of different M/VG nanoparticles were measured and optimized using a Zetasizer (Nano ZS, Malvern Instruments, UK). The hydrodynamic size of the optimized M/VG nanoparticles was examined using dynamic light scattering (BT-90, Bettersize Instruments Ltd., China). Transmission electron microscopy (TEM) was used to observe the morphology of the optimized M/VG nanoparticles (JEM-2100, JEOL Ltd., Japan). Each experiment was repeated thrice.

Circular dichroism (CD) spectrum analysis

The CD spectra of free melittin and M/VG nanoparticles were analyzed at the same concentration of melittin (0.5 mg/mL) in a quartz cell at 200 to 280 nm with a path length of 0.1 cm. Each group was examined thrice.

Hemolysis evaluation

The whole blood of rats was obtained and centrifuged at $3000 \times g$ for 10 min to collect red blood cells (RBCs). Then melittin or M/VG nanoparticles at various concentrations were added to the 2×10^8 RBC/mL suspension, incubated at 37 °C, centrifuged at $1000 \times g$ for 5 min, and further analyzed using a microplate reader at 410 nm. Each group was examined thrice.

MTT assay

The MTT assay was used to evaluate the anti-tumor effect on HepG2 cells in vitro. Briefly, HepG2 cells were seeded in 96-well plates, cultured for 24 h, and incubated with melittin or M/VG nanoparticles for another 48 h. Then MTT solution was added, and the cells were cultured for another 4 h. Finally, after removal of the medium, DMSO was added to each well and the absorbance was measured at 570 nm using a microplate reader. Each group was examined six times.

Wound healing experiment

HepG2 cells were seeded in 24-well plates and cultured for 12 h. Next, the HepG2 cells were scratched using a 20 μL micropipette tip to form wounds. This was recorded as 0 h. Then the cells were treated with a different group for 48 h. Wound images were recorded and evaluated at both 0 and 48 h. Each group was examined thrice.

Apoptosis assay

HepG2 cells were cultured for 24 h and incubated with free medium, melittin, or M/VG nanoparticles. After 48 h, the cells were digested with trypsin, washed with phosphate-buffered saline, stained using an apoptosis detection kit, and analyzed using flow cytometry. Each group was examined thrice.

In vivo imaging

The HepG2 cells (5×10^6/mL) were collected in a serum-free RPMI-1640 medium (200 μL) and subcutaneously injected into the right forelimb axilla of BALB/c nude mice. When tumor volumes grew to approximately 150 mm^3, Cy5-labeled melittin or Cy5-labeled nanoparticles ($n = 3$) were intravenously injected into BALB/c mice via the tail vein. After injection, the fluorescent signal of Cy5 was recorded at 1, 2, 4, 8, and 24 h

with an IVIS 200 imaging system (PerkinElmer, Hopkinton, MA, USA). Tumor tissues and major organs were obtained and observed at the end of the experiments using an optical imaging platform.

In vivo anti-tumor effect and safety evaluation

To further explore the therapeutic effect in vivo, the HepG2 cells (5×10^6 /mL) were collected in a serum-free RPMI-1640 medium (200 μL) and subcutaneously injected into the right forelimb axilla of BALB/c nude mice. Mice were divided into five groups ($n = 5$) when tumor volumes reached 50 mm^3. Four groups were injected a total of four doses of saline (blank control), melittin (2.5 mg/kg), M/VG nanoparticles (2.5 mg/kg), or M/VG nanoparticles (5 mg/kg) via the tail vein every 3 days. The positive control was orally administered a total of 12 doses of sorafenib (30 mg/kg) daily. Tumor size was calculated once in every 3 days.

After treatment, tumor tissues and the major organs were collected for further hematoxylin and eosin (H&E) or Ki67 analysis. Fresh blood was further analyzed, and biochemical parameters were measured.

Statistical analysis

All data are shown as mean ± standard deviation and further analyzed using the student's t test. Differences were considered significant at $P < 0.05$.

Results and discussion

Self-assembly mechanism

The structures of melittin and VG are shown in Fig. 1A. MD simulation snapshots depict the time evolution between melittin and VG. Initially, melittin and VG aggregated within 3 ns. The self-assembled nanoparticles became stable after 6 ns, as shown in Fig. 1B.

In the designed self-assembly system, the interaction was mainly composed of hydrogen bonds (Fig. 1C) and stacking effects (Fig. 1D). The Van der Waals force in M/VG nanoparticles declined significantly with MD simulations, gradually stabilized after 6 ns, and stabilized in the range of −2000 kJ/mol, indicating that the stacking effect (dominated by Van der Waals force) in the designed self-assembly gradually strengthened (Fig. 2A). Figure 2B shows changes in the number of hydrogen bonds during the self-assembly process. In the first 6 ns, there were approximately ten
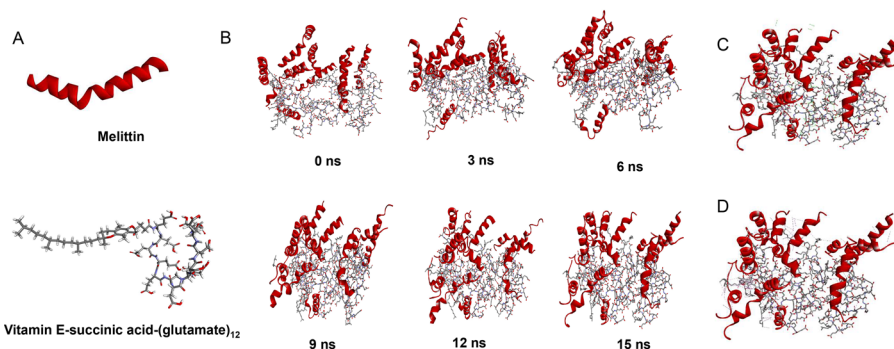

Fig. 1 Structures of melittin and VG (**A**) and its MD simulation for 15 ns (**B**). In the designed self-assembly system, the interaction is mainly composed of hydrogen bonds (**C**) and stacking effects (**D**)
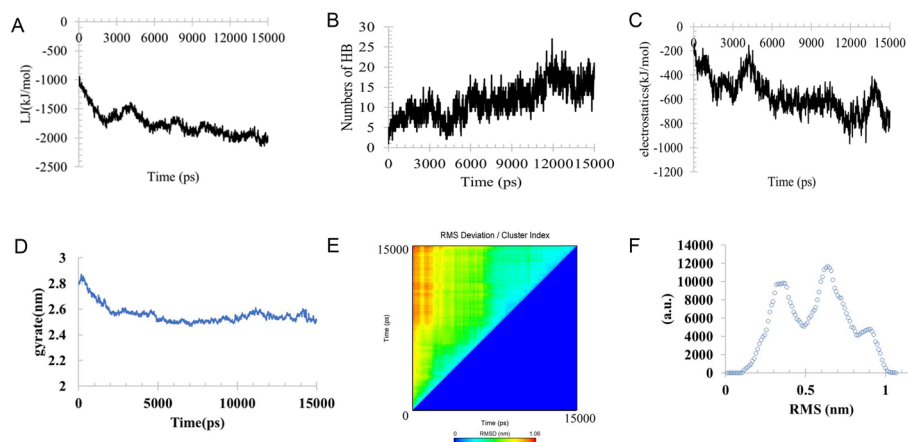
Fig. 2 Change in Van der Waals force (**A**), hydrogen bonds (**B**), and electrostatic force energy (**C**), radius of gyration (**D**), root-mean-square deviation (**E**), and cluster behavior (**F**) in the self-assembly process

intermolecular hydrogen bonds in the designed system. When simulated from 6 to 12 ns, the number of hydrogen bonds increased from 10 to 12 and stabilized. After 12 ns, the number of hydrogen bonds further increased and stabilized at 15–20. The electrostatic force energy (Fig. 2C) showed the same trend as the number of hydrogen bonds; as the number of hydrogen bonds increased, the electrostatic force energy gradually stabilized.

In the first 3 ns, the radius of gyration decreased significantly from approximately 2.8 nm to 2.6 nm. After approximately 3 ns, the radius of gyration of the t-system gradually stabilized. The results show that the system was assembled successfully after 3 ns (Fig. 2D).

Figure 2E indicates that in the first 3 ns, the root-mean-square deviation (RMSD) of the clustering system was the largest at approximately 1.0 nm. From 3 to 8 ns, the RMSD between cluster systems decreased to approximately 0.7 nm. After 8 ns, the RMS deviation between clustering systems gradually tended to 0.4 nm. These results confirmed that with the advancement of simulation time, the RMS deviation in clusters gradually decreased, resulting in self-assembly behavior and finally forming a stable nanoparticle structure. The results are consistent with the cluster behavior shown in Fig. 2F.

After forming a stable structure, the interactions between melittin and VG (Fig. 3A) were mainly based on hydrogen bonds and stacking interactions. GLY3, ALA4, and VAL5 in melittin interacted with the carbonyl or carboxyl of glutamate in VG via hydrogen bonding through NH–O interactions. LEU9 in melittin interacted with the benzene ring of vitamin E in VG by stacking interactions through CH–π interactions. ILE2 and VAL5 in melittin interacted with the benzene ring of vitamin E in VG by stacking interactions through CH–CH interactions. The interactions between VG and VG (Fig. 3B) were also mainly based on hydrogen bonds (OH–O and OH–N between glutamates) and stacking interactions (CH3–π and CH3–CH3 between vitamin E). The interactions between melittin and melittin (Fig. 3C) were also mainly based on hydrogen bonds (THR10 with PRO14 or SER18 by OH–O, LEU6 with SER18 by O–HO) and stacking interactions (LEU9-ILE17, PRO14-PRO14, and SER18-LEU6).
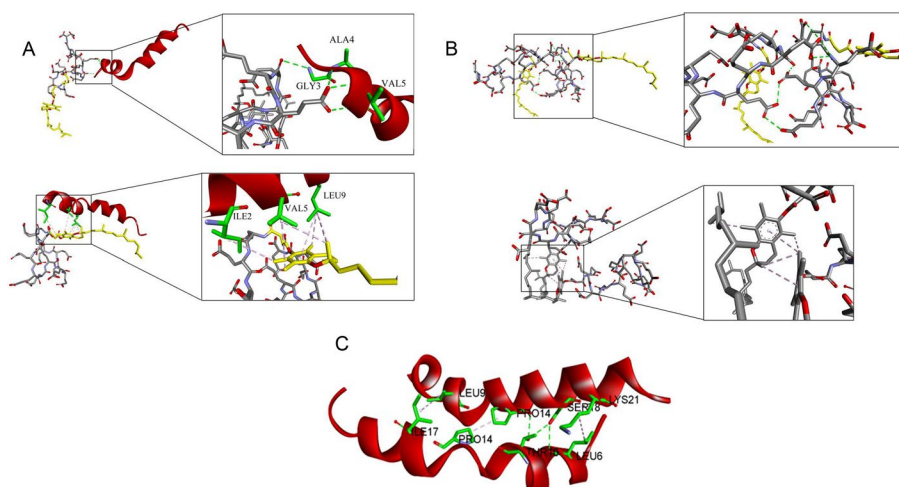
Fig. 3 Interactions between melittin and VG (**A**), VG and VG (**B**), melittin and melittin (**C**) mainly based on hydrogen bonds (green) and stacking interaction (pink)
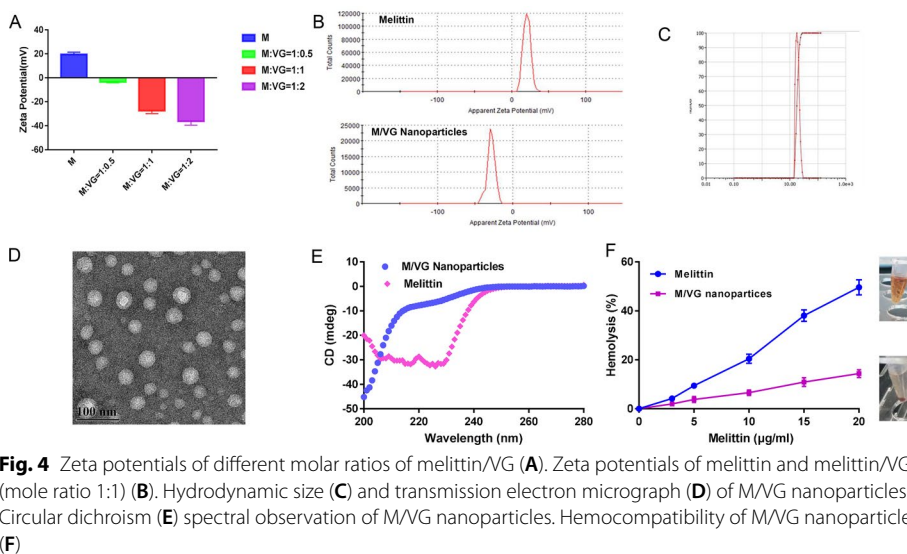

Fig. 4 Zeta potentials of different molar ratios of melittin/VG (**A**). Zeta potentials of melittin and melittin/VG (mole ratio 1:1) (**B**). Hydrodynamic size (**C**) and transmission electron micrograph (**D**) of M/VG nanoparticles. Circular dichroism (**E**) spectral observation of M/VG nanoparticles. Hemocompatibility of M/VG nanoparticles (**F**)

Characterization of M/VG nanoparticles

We optimized the mole ratio of melittin to VG in the self-assembly by zeta potentials, as shown in Fig. 4A. This was conducted because shielding the positive charges of melittin is essential to decrease its hemolysis. With an increase in VG, the electric charge of self-assembled nanoparticles was reversed. To optimize the self-assembled nanoparticles of melittin and VG (mole ratio, 1:1), the potential of melittin (+19.6 mV) was transformed into −26.8 mV, which was selected owing to the stable negative potential (Fig. 4B). The surface charge of M/VG nanoparticles was negative, which helped the self-assembled particles to escape from the recognition of the reticuloendothelial system, increasing the retention time in vivo (Cheng et al. 2014). The hydrodynamic size of the M/VG nanoparticles was 63.4 nm with a polydispersity

index of 0.193 (Fig. 4C). As shown in Fig. 4D, the M/VG nanoparticles are spherical particles sized approximately 30 nm. TEM revealed that the nanoparticles had smaller hydrodynamic size, which may be because TEM assesses solid particle sizes excluding the water layer, unlike the hydrodynamic size. The average sizes of M/VG nanoparticles were smaller than the inter-endothelial gaps in most tumor vessels (380–780 nm), which are small enough to passively permeate into the tumor (Chen et al. 2016; Jain and Stylianopoulos 2010).

CD spectrum characteristics

The CD spectra in Fig. 4E reveal that melittin has an α-helical configuration with negative peaks at approximately 209 and 220 nm. The results also demonstrated that VG converts the conformation of melittin because of the random coil of the M/VG nanoparticles. Previous reports suggested that melittin has an α-helical structure that easily binds to lipid membranes (Toraya et al. 2004; Lundquist et al. 2008). Therefore, the change in the α-helical signal into a random coil suggests that M/VG nanoparticles might have low hemolysis. Furthermore, VG could stabilize an existing random coil structure other than melittin.

Hemocompatibility of M/VG nanoparticles

As mentioned above, VG promoted the electric charge conversion of melittin by self-assembly (Fig. 4B). Shielding the positive charge of melittin is crucial for decreasing the interaction with RBCs (Zhou et al. 2021b). Furthermore, after self-assembly into M/VG nanoparticles, the α-helical melittin changed into a random coil, probably yielding a decreased hemolytic effect of melittin (Fig. 4E). In vitro hemolytic evaluation indicated that melittin at a concentration of 20 μg/mL could lyse almost 50% RBCs, whereas it only exhibited 12% hemolysis (Fig. 4F) at equal concentrations in M/VG nanoparticles, further confirming that the fabricated self-assembly could remarkably increase the hemocompatibility of melittin.

MTT assay

The MTT assay was performed to evaluate the anti-tumor effect on HepG2 cells in vitro. The relative results indicated that the viability of melittin and M/VG nanoparticles-treated cells decreased significantly as the concentration of melittin increased (Fig. 5A). Meanwhile, the half-maximal inhibitory concentration (IC_{50}) of M/VG nanoparticles was calculated as 2.13 μg/mL, i.e., a decrease of 55.16%, compared with that of melittin (4.75 μg/mL). This could be attributed to the different cellular uptake mechanisms of melittin and M/VG nanoparticles in HepG2 cells. Designed M/VG nanoparticles have good hemocompatibility and effective therapeutic impact.

Apoptosis assay

HepG2 cells in the control group exhibited low apoptosis levels, as shown in Fig. 6A. Conversely, the M/VG nanoparticles significantly induced apoptosis in HepG2 cells which increased by 14.6%, compared with the melittin group (Fig. 5B).
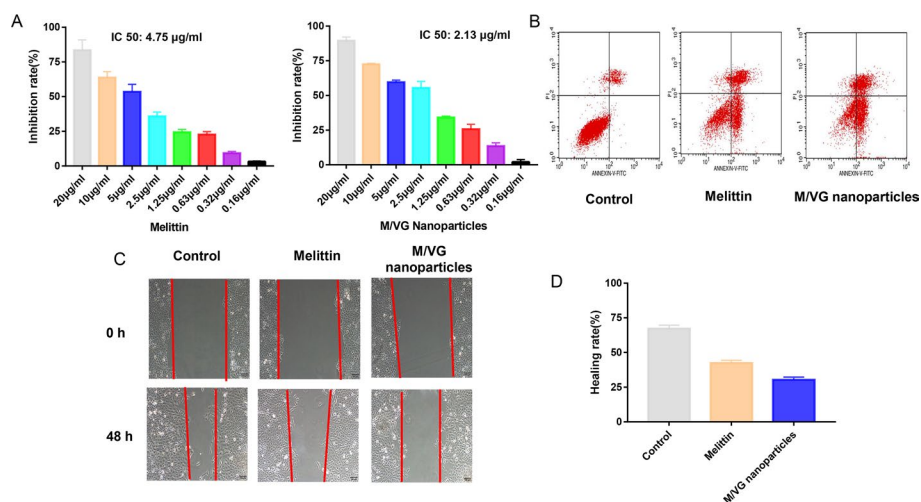
Fig. 5 Viability (**A**) and apoptosis analysis (**B**) of HepG2 cells after treatment with melittin or M/VG nanoparticles for 48 h. Motility (**C**) and quantitative analysis of healing rate for melittin or M/VG nanoparticles (**D**)
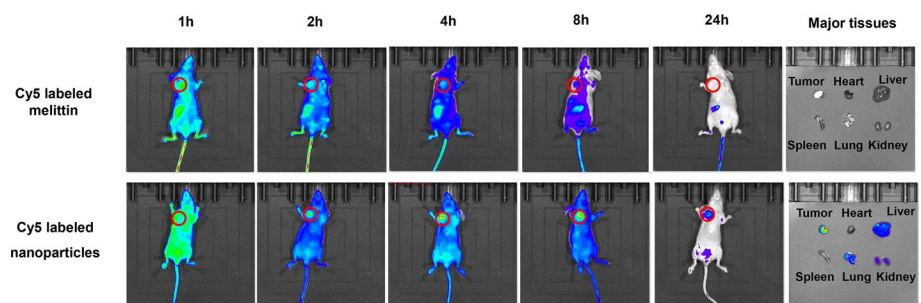

Fig. 6 In vivo targeted imaging of Cy5-labeled melittin and Cy5-labeled nanoparticles

Wound healing assay

The effect of M/VG nanoparticles on HepG2 cell motility was evaluated using a scratch wound healing assay. As shown in Fig. 5C and D, HepG2 cells in the control group showed a significant motor aggregation phenotype. Both melittin and M/VG nanoparticles significantly inhibited cell motility. Compared with the melittin group, M/VG nanoparticles presented a lower healing rate, which further decreased by 28.41%.

In vivo imaging

To assess the tumor-targeting capability of Cy5-labeled nanoparticles, biodistributions of Cy5-labeled melittin and Cy5-labeled nanoparticles were monitored. As shown in Fig. 6, Cy5-labeled melittin had insufficient tumor-targeting capacity and non-specific distribution. Conversely, Cy5-labeled nanoparticles first presented a fluorescence signal at 2 h in the tumor location after injection. As time elapsed, stronger fluorescent signals in the tumor region reached a plateau at 4 h. Notably, the Cy5-labeled nanoparticles were stably retained in the tumors and could be detected after 24 h, validating a significant systemic long circulation and tumor-targeting capacity. Meanwhile, the ex vivo

fluorescence imaging of tumor tissues and main organs as shown in Fig. 6 also indicated that Cy5-labeled nanoparticles could increase the accumulation of melittin in tumors, which is consistent with the in vivo imaging results. Furthermore, only lower deposition was detected in the liver, lung, and kidney. More importantly, Cy5-labeled nanoparticles showed a longer liver retention time, which may have potential application in hepatocellular carcinoma. Notably, rapid clearance was found for the Cy5-labeled melittin, and fluorescence signals of the Cy5-labeled melittin group were less than those of the Cy5-labeled nanoparticles group, especially in the tissues after 24 h.

In vivo anti-tumor evaluation

Owing to the decreased hemolysis in vitro and increased tumor accumulation in vivo, an in vivo anti-tumor evaluation was performed. Limited tumor growth inhibition (39.86%) of melittin was observed, which could be attributed to the rapid clearance of the injections in the circulation system and lower affinity with the HepG2 cells. Compared to the melittin group, the self-assembled nanoparticles showed a longer retention time and specific tumor permeation (Fig. 6). As expected, the tumor growth curve and tumor images showed that M/VG nanoparticles dramatically suppressed tumor growth (Fig. 7A and B). At the end of the experiments, compared with the control group, mice treated with M/VG nanoparticles showed a 70.19% decrease in tumor volume for M/VG nanoparticles (2.5 mg/kg) and 92.96% inhibition against M/VG nanoparticles (5 mg/kg). Additionally, compared to the sorafenib group (positive control), the M/VG nanoparticles (5 mg/kg) group showed a dramatic decrease of 60.42% in tumor size. When treated with melittin (2.5 mg/kg), hemolysis began from the bottom of the caudal vein, and melittin was gradually injected from the bottom to the top of the mouse tail. Therefore, the tails of mice in the melittin (2.5 mg/kg) group showed severe tissue necrosis. Interestingly, the M/VG nanoparticle group exhibited no significant tail injury, even at a high dose of 5 mg/kg (Fig. 7C).

H&E and Ki67 staining of tumor tissues were used for histological evaluation (Fig. 7D). In the control group, tumor cells were large, polygonal, or almost round with obvious
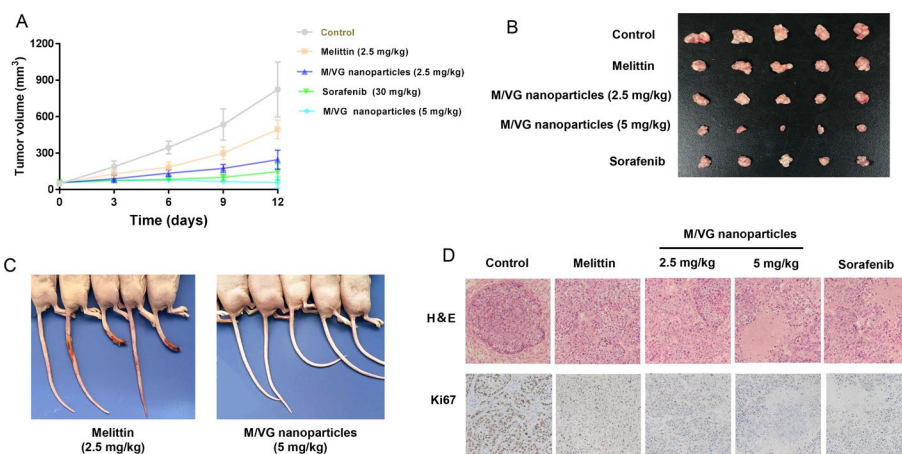

Fig. 7 Tumor growth curve (**A**) and tumor images at the end of the experiment (**B**) for different treatments. Tail injury observation of melittin (2.5 mg/kg) and M/VG nanoparticles (5 mg/kg) at the end of the experiments (**C**). H&E and Ki67 staining of tumor tissues (**D**)

nucleoli and were easily observed. Fibrous tissues divided the tumor cells into small nests. For melittin and M/VG nanoparticles (2.5 mg/kg) groups, tumor cells were distributed diffusely without significant nest structure. Furthermore, when treated with M/VG nanoparticles (5 mg/kg) or sorafenib, tumor cells died significantly with no nuclear and dull cytoplasm eosin staining. Ki67 is a marker of tumor cell proliferation. The proportion of Ki67 positive cells in the control group was significantly higher than that in the M/VG nanoparticles (5 mg/kg) group. The results showed that treatment with M/VG nanoparticles (5 mg/kg) induced malignant hepatoma proliferation (Fig. 7D).

Additionally, for histological evaluation, compared with the control, there were no significant histological changes in the major tissues in other treatment groups (Fig. 8). Meanwhile, melittin caused a significant decrease in hematocrit, demonstrating that melittin interacts with hemocytes in vivo; however, M/VG nanoparticles exhibited similar hemocyte levels as the control group. These results collectively indicate that M/VG nanoparticles can be used safely without the development of evident hematotoxicity (Fig. 9).

Forming nanocarriers to reduce hemolysis and understanding their passive tumor-targeting distribution via the enhanced permeation and retention effect can be used to improve the effect of melittin. Different materials, such as cypate (Jia et al. 2019), chlorin e6 (Jia et al. 2018), condensed epigallocatechin gallate (Qiao et al. 2018), γ-polyglutamic acid (Ye et al. 2021), and large pores mesoporous silica nanoparticles (Yu et al. 2020) are assembled with melittin. Compared to previously reported self-assembly systems of melittin, this plain system consists of peptides sourced from amino acids (the basic structure of the human body), which could be administered in high does, increasing the dosage in vivo. Furthermore, distinctive morphology of M/VG nanoparticles was
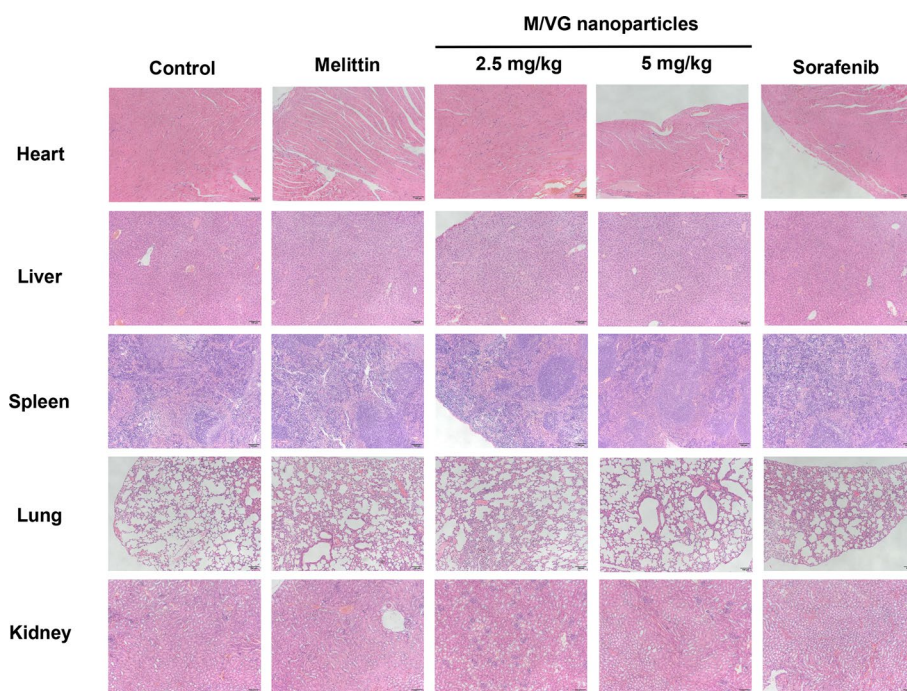

Fig. 8 H&E of the heart, liver, spleen, lung, and kidney for in vivo anti-tumor evaluation of all groups
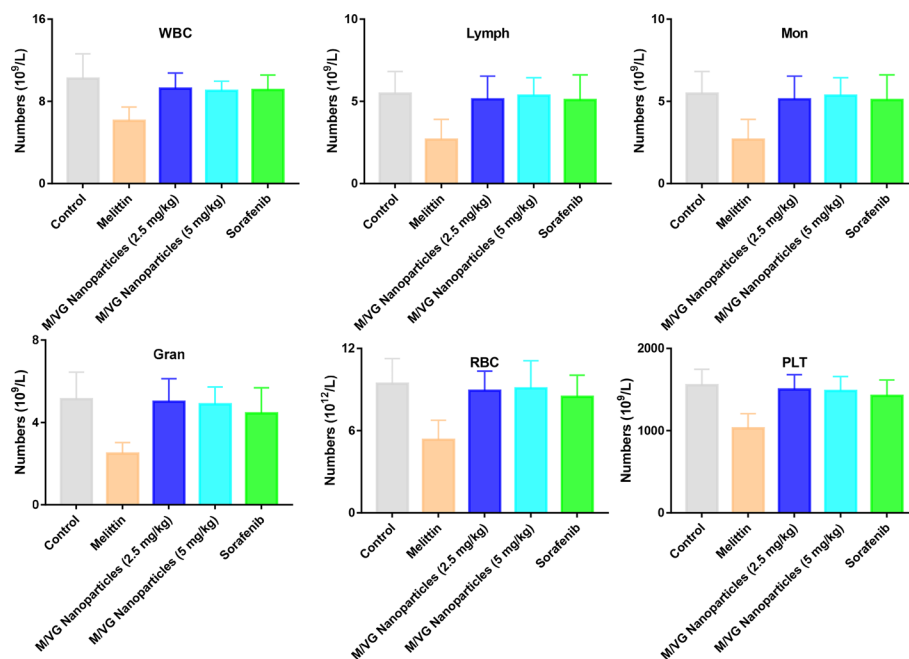
Fig. 9 Hemocyte levels of all groups at the end of in vivo anti-tumor evaluation

simulated and is shown in Fig. 1B. Self-assembly interaction, which was mainly composed of hydrogen bonds and stacking effects, was explained using MD simulations.

M/VG nanoparticles can decrease hemolysis, increase the accumulation in tumor tissues, and exhibit effective anti-tumor effects against HepG2 cells with no significant histological changes in major tissues. We aim to further analyze the possible difference between melittin and M/VG nanoparticles on tumor cell membrane disruption using coarse-grained simulation and atomic force microscopy observation.

Furthermore, melittin as antibiotic peptide also can be used for exploring the wound healing effects. Postsurgical tumor patients' treatments are often performed after wound healing. The delay in adjuvant therapy could prevent destruction of the residual tumor cells. Our previous studies indicated that the chitosan hybrid hydrogel systems could load drugs and exhibit hemostasis; they were antibacterial and promoted wound healing (Jin et al. 2020, 2021). Based on our previous research, we aim to design in situ gel-forming chitosan hybrid hydrogel systems containing melittin self-assembly nanoparticles to promote wound healing, activate immunity, and prevent recurrence.

Tumor patients could be treated immediately after surgery, which could fill the gap between surgery and chemotherapy before wound healing. To explore the mechanism of chitosan hybrid thermosensitive hydrogel loading the melittin self-assembled nanoparticles more elaborately, we intend to analyze the forming mechanism using MD simulation. Hemostasis, antibacterial action, wound healing, apoptosis, activation of immune system, and recurrence require further research.

We anticipate that intended study could effectively prevent postsurgical recurrence by multiple functions. Establishment of this platform could be treated immediately after surgery, which fill gaps between surgery and chemotherapy before wound healing, has potential applicability in clinical treatment.

Jin *et al. Cancer Nanotechnology*   (2023) 14:2

Page 13 of 14

Conclusion

Melittin was self-assembled with VG to form nanoparticles using a simple environment-friendly preparation method. Melittin interacted with VG on the surface of spherical nanoparticles via hydrogen bond interactions and π–π stacking interactions. In vivo imaging revealed that melittin accumulation in HepG2 cells significantly increased after self-assembly. Importantly, after formation of the M/VG nanoparticles, compared with free melittin, hemolysis decreased significantly and the dosage administration increased remarkably. Therefore, M/VG nanoparticles (5 mg/kg) exhibited superior anti-tumor effects against HepG2 cells by promoting apoptosis both in vitro and in vivo. Tumor volumes decreased by 92.96% compared with the control, indicating a potential therapeutic effect. In contrast to previously reported melittin systems, our research supports a simple and promising self-assembling system using natural bioactive peptides for targeted precision therapy, particularly to employ toxicants in safe therapeutic systems.

Abbreviations

VG	Vitamin E-succinic acid-(glutamate)12
M/VG	Melittin and vitamin E-succinic acid-(glutamate)12 self-assembly
TEM	Transmission electron microscopy
CD	Circular dichroism
RBC	Red blood cells
H&E	Hematoxylin and eosin
MD	Molecular dynamics
RMSD	Root-mean-square deviation

Declarations

Ethics approval and consent to participate
All animal experiments were approved by the Animal Ethics Committee of Jiangsu Province Academy of Traditional Chinese Medicine.

Consent for publication
All authors provided consent for publication.

Competing interests
The authors declare that they have no competing interests.

References
Bian T, Gardin A, Gemen J, Houben L, Perego C, Lee B, Elad N, Chu ZL, Pavan GM, Klajn R (2021) Electrostatic co-assembly of nanoparticles with oppositely charged small molecules into static and dynamic superstructures. Nat Chem 13:940–949

Chen L, Lian JF (2013) Peptide fibrils with altered stability, activity, and cell selectivity. Biomacromol 14(7):2326–2331

Chen G, Roy I, Yang C, Prasad PN (2016) Nanochemistry and nanomedicine for nanoparticle-based diagnostics and therapy. Chem Rev 116(5):2826–2885

Cheng B, Xu P (2020) Redox-sensitive nanocomplex for targeted delivery of melittin. Toxins 12:582–594

Cheng B, Thapa B, Remant KC, Xu PS (2014) Dual secured nano-melittin for the safe and effective eradication of cancer cells. J Mater Chem B Mater Biol Med 3(1):25–29

Du G, He P, Zhao J, He C, Sun X (2021) Polymeric microneedle-mediated transdermal delivery of melittin for rheumatoid arthritis treatment. J Control Release 336:537–548

Green BD, Gault VA, Mooney MH, Irwin N, Harriott P, Greer B, Bailey CJ, O'Harte FP, Flatt PR (2004) Degradation, receptor binding, insulin secreting and antihyperglycaemic actions of palmitate-derivatised native and Ala8-substituted GLP-1 analogues. Biol Chem 385(2):169–177

Jain RK, Stylianopoulos T (2010) Delivering nanomedicine to solid tumors. Nat Rev Clin Oncol 7(11):653–664

Jia HR, Zhu YX, Xu KF, Wu FG (2018) Turning toxicants into safe therapeutic drugs: cytolytic peptide photosensitizer assemblies for optimized in vivo delivery of melittin. Adv Healthc Mater 7(16):1800380

Jia HR, Zhu YX, Liu X, Pan GY, Wu FG (2019) Construction of dually responsive nanotransformers with nanosphere–nanofiber–nanosphere transition for overcoming the size paradox of anticancer nanodrugs. ACS Nano 13(10):11781–11792

Jin X, Fu Q, Gu ZH, Zhang ZH, Lv HX (2020) Injectable corilagin/low molecular weight chitosan/PLGA-PEG-PLGA thermosensitive hydrogels for localized cancer therapy and promoting drug infiltration by modulation of tumor microenvironment. Int J Pharm 589:119772

Jin X, Fu Q, Gu ZH, Zhang ZH, Lv HX (2021) Chitosan/PDLLA-PEG-PDLLA solution preparation by simple stirring and formation into a hydrogel at body temperature for whole wound healing. Int J Biol Macromol 184:787–796

Kim W (2021) Bee venom and its sub-components: characterization, pharmacology, and therapeutics. Toxins 13:191

Kim JE, Park YJ (2022) Hyaluronan self-agglomerating nanoparticles for non-small cell lung cancer targeting. Cancer Nano. https://doi.org/10.1186/s12645-022-00115-0

Lai YT, King NP, Yeates TO (2012) Principles for designing ordered protein assemblies. Trends Cell Biol 22:653–661

Li YW, Xu N, Zhu WH, Wang L, Liu B, Zhang JX, Xie ZG, Liu WS (2018) Nanoscale melittin@zeolitic imidazolate frameworks for enhanced anticancer activity and mechanism analysis. ACS Appl Mater Interfaces 10(27):22974–22984

Lundquist A, Wessman P, Rennie AR, Edwards K (2008) Melittin–lipid interaction: a comparative study using liposomes, micelles and bilayerdisks. Biochim Biophys Acta 1778:2210

Lv S, Sylvestre M, Song K, Pun SH (2021) Development of d-melittin polymeric nanoparticles for anti-cancer treatment. Biomaterials 277(73):121076

Lyu C, Fang F, Li B (2018) Anti-tumor effects of melittin and its potential applications in clinic. Curr Protein Pept Sci 19(3):240–250

Mao J, Liu S, Ai M, Wang Z, Wang D, Li X, Hu K, Gao X, Yang Y (2017) A novel melittin nano-liposome exerted excellent anti-hepatocellular carcinoma efficacy with better biological safety. J Hematol Oncol 10(1):71–74

Motiei M, Aboutalebi F, Forouzanfar M, Dormiani K, Mirahmadi-Zare SZ (2021) Smart co-delivery of mir-34a and cytotoxic peptides (ltx-315 and melittin) by chitosan based polyelectrolyte nanocarriers for specific cancer cell death induction. Mat Sci Eng c 128:112258

Peeler DJ, Thai SN, Cheng Y, Horner PJ, Sellers DL, Pun SH (2019) pH-sensitive polymer micelles provide selective and potentiated lytic capacity to venom peptides for effective intracellular delivery. Biomaterials 192:235–244

Qiao HZ, Dong F, Lei Z, Gu X, Di L (2018) Nanostructured peptidotoxins as natural pro-oxidants induced cancer cell death via amplification of oxidative stress. ACS Appl Mater Interfaces 10(5):4569–4581

Sung H, Ferlay J, Siegel RL, Laversanne M, Soerjomataram I, Jemal A, Bray F (2021) Global cancer statistics 2020: GLOBOCAN estimates of incidence and mortality worldwide for 36 Cancers in 185 Countries. CA Cancer J Clin 71(3):209–249

Toraya S, Nishimura K, Naito A (2004) Dynamic structure of vesicle-bound melittin in a variety of lipid chain lengths by solid-state NMR. Biophys J 87:3323–3335

Tu Z, Hao J, Kharidia R, Meng XG, Liang JF (2007) Improved stability and selectivity of lytic peptides through self-assembly. Biochem Biophys Res Commun 361(3):712–717

Ventura CR, Wiedman GR (2021) Substituting azobenzene for proline in melittin to create photomelittin: A light-controlled membrane active peptide. Biochem Biophys Acta 1863(12):183759

Wang Y, Zhang X, Wan K et al (2021) Supramolecular peptide nano-assemblies for cancer diagnosis and therapy: from molecular design to material synthesis and function-specific applications. J Nanobiotechnol 19:253–284

Ye R, Zheng Y, Chen Y, Wei XH, Shi SY, Chen YT, Zhu WX, Wang AQ, Yang LX, Xu YH, Peng JL (2021) Stable loading and delivery of melittin with lipid-coated polymeric nanoparticles for effective tumor therapy with negligible systemic toxicity. ACS Appl Mater Interfaces 13:55902–55912

Yu QL, Deng T, Lin FC, Zhang B, Zink JI (2020) Supramolecular assemblies of heterogeneous mesoporous silica nanoparticles to co-deliver antimicrobial peptides and antibiotics for synergistic eradication of pathogenic biofilms. ACS Nano 14:5926–5937

Zhou YH, Ye T, Ye CZ, Wan C, Yuan SY, Liu YS, Li TY, Jiang FG, Lovell JF, Jin HL, Chen J (2021a) Secretions from hypochlorous acid-treated tumor cells delivered in a melittin hydrogel potentiate cancer immunotherapy. Bioact Mater 9:541–553

Zhou J, Wan C, Cheng J, Huang H, Jin H (2021b) Delivery strategies for melittin-based cancer therapy. ACS Appl Mater Interfaces 13(15):17158–17173

Publisher's Note